Eurasia Specialized Veterinary Publication

International Journal of Veterinary Research and Allied Science

ISSN:3062-357X

2024, Volume 4, Issue 1, Page No: 157-171

Available online at: www.esvpub.com/

Altered Platelet Activation Gene Expression in Dogs Affected by Stage B2 Myxomatous Mitral Valve Disease

Claire Jeannet[1]*, Laurent Simon[1]

[1]Department of Clinical Veterinary Sciences, Faculty of Veterinary Medicine, University of Montreal, Montreal, Canada.

***E-mail** ✉ c.jeannet.vet@yahoo.com

ABSTRACT

Peripheral blood contains numerous mRNAs that have the potential to influence cardiac physiology. Although stage B2 Myxomatous Mitral Valve Disease (MMVD) is known to involve prolonged hemodynamic stress and remodeling of cardiac chambers due to mitral regurgitation, the gene-expression alterations present in the blood of affected dogs have not yet been clearly defined. To explore these changes, we compared the blood transcriptomes of healthy dogs (NC) with those of dogs naturally diagnosed with stage B2 MMVD. High-throughput sequencing followed by Weighted Gene Co-expression Network Analysis (WGCNA) and functional enrichment analyses (GO and KEGG) revealed a "turquoise" gene module that showed the strongest association with echocardiographic measurements. Within this module, 64 genes were differentially expressed and predominantly mapped to pathways involved in platelet activation. From these, five genes—MDM2, ROCK1, RIPK1, SNAP23, and ARHGAP35—were chosen for further examination. qPCR validation showed that four of them (MDM2, ROCK1, RIPK1, and SNAP23) displayed significant expression differences ($P < 0.01$) between MMVD and control dogs. Additionally, correlation analyses indicated that these four genes were inversely related to several cardiac structural indices, mirroring the trends observed in the WGCNA output. Our investigation highlights four platelet activation–associated genes—MDM2, ROCK1, RIPK1, and SNAP23—as potential blood-based biomarkers for identifying stage B2 MMVD. These results enhance understanding of the molecular changes accompanying early disease progression.

Keywords: Dog, Myxomatous mitral valve, Biomarkers, Transcriptomic, *MDM2*

Received: 19 January 2023
Revised: 28 April 2024
Accepted: 03 May 2024

How to Cite This Article: Jeannet C, Simon L. Altered Platelet Activation Gene Expression in Dogs Affected by Stage B2 Myxomatous Mitral Valve Disease. Int J Vet Res Allied Sci. 2024;4(1):157-71.
https://doi.org/10.51847/ULJvpPiguF

Background

Myxomatous mitral valve disease (MMVD) is the most prevalent acquired cardiac disorder in dogs and represents approximately 75%–80% of heart disease cases in small breeds weighing
20 kg or less, such as Poodles, Cavalier King Charles Spaniels, and Chihuahuas [1, 2]. The resulting mitral regurgitation (MR) produces sustained volume overload, leading to enlargement of the left atrium, eccentric hypertrophy of the left ventricle, and progressive remodeling of the mitral valve, often accompanied by leaflet prolapse [2, 3]. While these structural adaptations may initially support cardiac output to meet metabolic needs, the disease ultimately advances, with congestive heart failure (CHF) being the typical indicator of transition to end-stage MMVD [4, 5]. Therefore, understanding the mechanisms driving these hemodynamic changes is crucial for developing preventive strategies.

Diagnosis commonly relies on a combined dynamic–static imaging approach using echocardiography and radiography, which together offer a more reliable assessment of cardiovascular disorders [6, 7]. Based on imaging variables—including normalized left ventricular internal diameter in diastole (LVIDDN), the left atrial-to-aortic ratio (LA:AO), and vertebral heart size (VHS)—the American College of Veterinary Internal Medicine (ACVIM) classifies MMVD into stages A through D. Stage B consists of dogs with identifiable structural abnormalities but no clinical symptoms and is further divided into B1 and B2 depending on whether cardiac remodeling is observed. Stage B2 marks the earliest detectable phase of remodeling and represents the point at which medical therapy is recommended to slow disease progression [2, 8]. However, both echocardiographic and radiographic evaluations require substantial time and are susceptible to inter-observer variability [9].

Several circulating molecules—including leptin, adiponectin, and NT-ProBNP—have been explored as potential biomarkers for MMVD [1, 10]. Nonetheless, elevations in leptin and adiponectin have been documented primarily in stage C rather than in stages A or B [1], and NT-ProBNP concentrations cannot reliably differentiate between stages B1 and B2 [10]. To date, no blood-based biomarker has been validated specifically for MMVD stage B2. Moreover, most omics investigations have focused on valvular tissues rather than blood [11–13], and transcriptomic correspondence between blood and tissue remains weak [14]. Existing biomarkers also suffer from limited specificity and may be influenced by non-cardiac conditions, reducing their diagnostic and prognostic value [15]. Consequently, there is a clear need for new peripheral biomarkers that can accurately identify stage B2 MMVD.

Rapid advancements in sequencing and computational technologies have positioned transcriptomics as an effective strategy for identifying novel biomarkers and exploring their functional roles [16, 17]. Compared with proteomic approaches, transcriptomic analyses generally offer greater sensitivity, increased reproducibility, and broader genome coverage [18]. Among transcriptomic tools, Weighted Gene Co-expression Network Analysis (WGCNA) is widely used for detecting gene modules associated with clinical phenotypes [19], and recent applications in cardiovascular research have provided important mechanistic insights [20, 21].

In this prospective study, we aimed to identify blood-based biomarkers for MMVD stage B2 in dogs. We applied WGCNA to determine gene modules linked to clinical traits and used Gene Ontology (GO) and Kyoto Encyclopedia of Genes and Genomes (KEGG) analyses to investigate the biological functions of differentially expressed genes (DEGs). Candidate biomarkers emerging from these analyses were first screened in a discovery cohort and subsequently validated through qPCR and correlation analyses. The findings contribute to identifying phenotype-associated DEGs and elucidating molecular pathways active during stage B2 MMVD, offering a new framework for studying disease mechanisms and developing genetic markers applicable to early-stage MMVD diagnosis.

Results

Animal characteristics

In the discovery cohort, dogs in the NC and MMVD groups showed no significant differences in sex distribution or body weight ($P > 0.05$). However, in the validation cohort, age differed significantly between NC and MMVD dogs ($P < 0.05$). Radiographic indicators—LA:AO, LVIDDN, and VHS—were significantly higher in stage B2 MMVD dogs than in NC dogs in both the discovery and validation cohorts.

Quality control and RNA sequencing assessment

Across the eight samples analyzed, sequencing produced 672.7 million raw reads (about 201.6 Gbps). After removing reads containing excessive N bases (more than 10%), low-quality reads, and adaptor sequences, 668.0 million high-quality clean reads remained (approximately 200.4 Gbps, with 23.1–27.7 Gbps per sample). Clean reads achieved mean Q20 and Q30 values above 98.3% and 95.2%, respectively. When aligned to the CanFam3.1 reference genome, 95.8% of reads from the NC group and 95.5% from the MMVD group successfully mapped to the Canis lupus familiaris genome, and GC content exceeded 56.4%. These metrics confirm that sequencing quality was high and suitable for downstream analyses.

Gene expression profiling

Gene expression was quantified based on transcript abundance using FPKM values. Overall, 25,464 genes were detected, including 884 newly annotated genes. In both NC and MMVD groups, 84.6% of genes showed low

expression (FPKM < 3), 12.9% displayed moderate expression (FPKM 3–60), and only 2.5% were highly expressed (FPKM > 60).

Using FPKM-based expression values from all eight samples, we calculated pairwise correlation coefficients and visualized them in a heat map **(Figure 1A)**. While expression correlations varied between groups, samples within the same group displayed highly similar patterns. To further assess grouping based on MMVD status, PCA was performed using all quantified transcripts. PC1 and PC2 accounted for 58.7% and 8.7% of the total variance, respectively, and clearly separated NC from MMVD samples, while showing tight clustering within each group **(Figure 1B)**. Altogether, the gene expression analyses confirm strong reproducibility among replicates and validate the suitability of the samples for differential expression analysis.

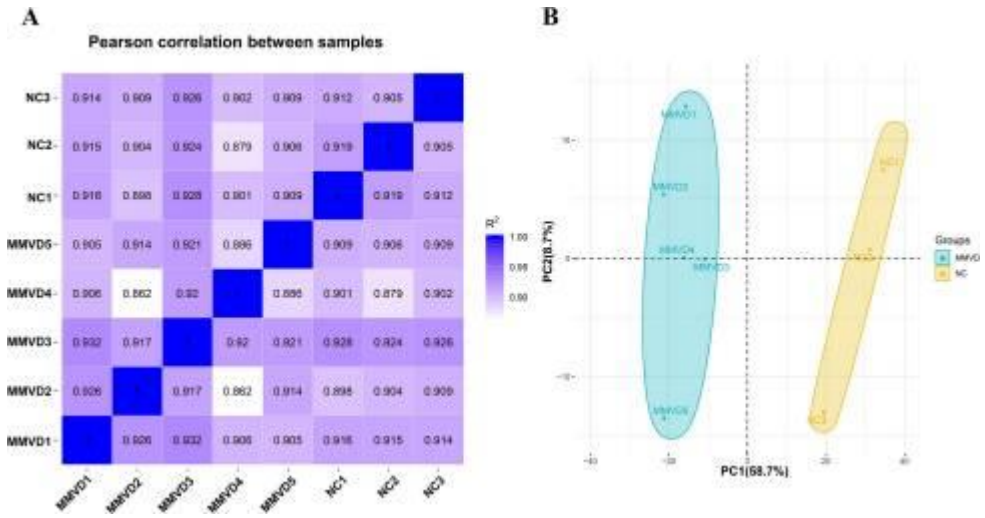

Figure 1. *Sample correlation and principal component analysis.* **A**. Heatmap depicting hierarchical clustering of all eight samples (3 NC and 5 MMVD) generated using Pearson correlation. Bolded numbers indicate the R^2 values (squared Pearson correlation coefficients) for the respective sample replicates. All correlations were highly significant ($P < 1\times10^{-16}$). **B**. PCA plot illustrating sample distribution. NC samples are shown as yellow triangles, while MMVD samples are represented as green circles. Each group is enclosed within a 95% confidence ellipse. The percentages on each axis correspond to the proportion of total variance explained

Weighted correlation network analysis

Weighted gene correlation network analysis (WGCNA) enables the identification of gene groups that change in a coordinated manner and allows exploration of how these gene clusters relate to specific phenotypic traits. To determine which gene modules were most strongly associated with MMVD-related clinical features, we applied WGCNA to the transcriptome dataset.

Clinical variables incorporated into the analysis included sex, age, and body weight, as well as radiologic measurements such as LA, AO, LA/AO ratio, LVIDDN, and VHS. Using a soft-thresholding power of 10 (scale-free $R^2 = 0.7$), the analysis generated 41 distinct gene modules, which are displayed in the cluster dendrogram in **Figure 2A–B**.

The module–trait correlation heatmap revealed eight modules with significant associations with at least one structural cardiac parameter **(Figure 2C)**. Among these, the turquoise module showed the strongest relationships: it was positively correlated with AO ($r = 0.80$, $P < 0.05$), and negatively correlated with LA ($r = –0.74$), LA:AO ($r = –0.92$), and LVIDDN ($r = –0.90$), all with $P < 0.05$. A moderate negative association with VHS was also observed ($r = –0.60$, $P < 0.05$). In contrast, correlations with sex, age, and body weight were weak ($r = –0.14$, –0.46, and 0.24, respectively; $P > 0.05$).

The turquoise module contained 1324 genes in total. Based on the intramodular connectivity (kWithin) values, we selected the top 100 genes as hub genes for subsequent analyses.

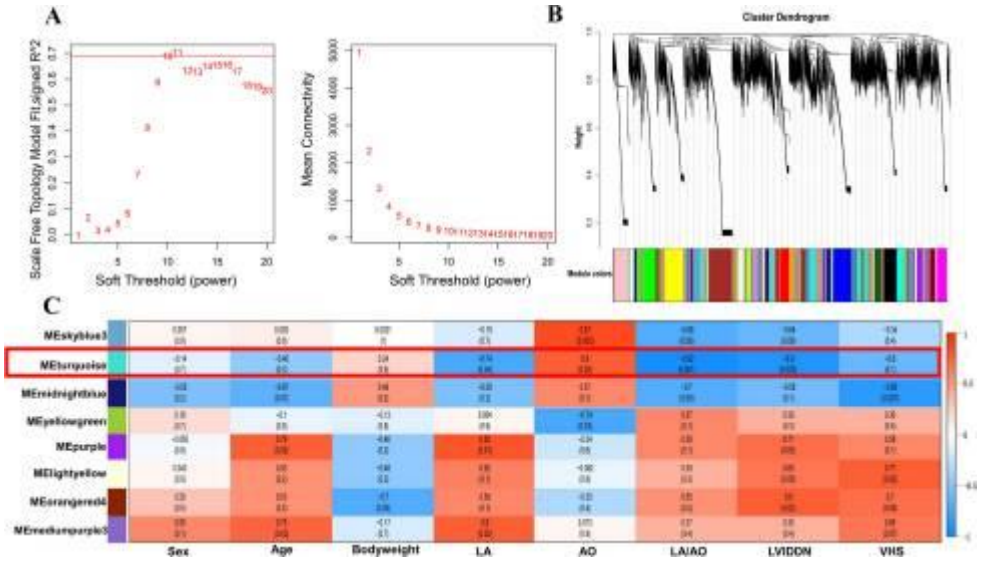

Figure 2. Identification of MMVD-associated modules using WGCNA. *A* Soft-thresholding analysis showing the scale-free topology fit (left) and mean connectivity (right) across different β values; *B* Gene clustering dendrogram generated from topological overlap measurements, with module assignments indicated by color; *C* Heatmap illustrating correlations between module eigengenes and MMVD clinical variables. Each cell reports the correlation coefficient alongside its corresponding P-value

Differentially expressed gene (DEG) analysis

Raw read counts from the transcriptome dataset were processed to determine differential expression. Genes meeting the criteria |log2 fold change| > 0 with $P < 0.05$ were classified as DEGs. In total, 990 DEGs were detected between healthy controls and MMVD dogs, comprising 934 annotated genes and 56 novel transcripts. Of these, 407 were upregulated and 583 were downregulated, as visualized in the volcano plot **(Figure 3A)**. A hierarchical clustering heatmap further demonstrated a clear separation in expression patterns between the NC and MMVD groups **(Figure 3B)**.

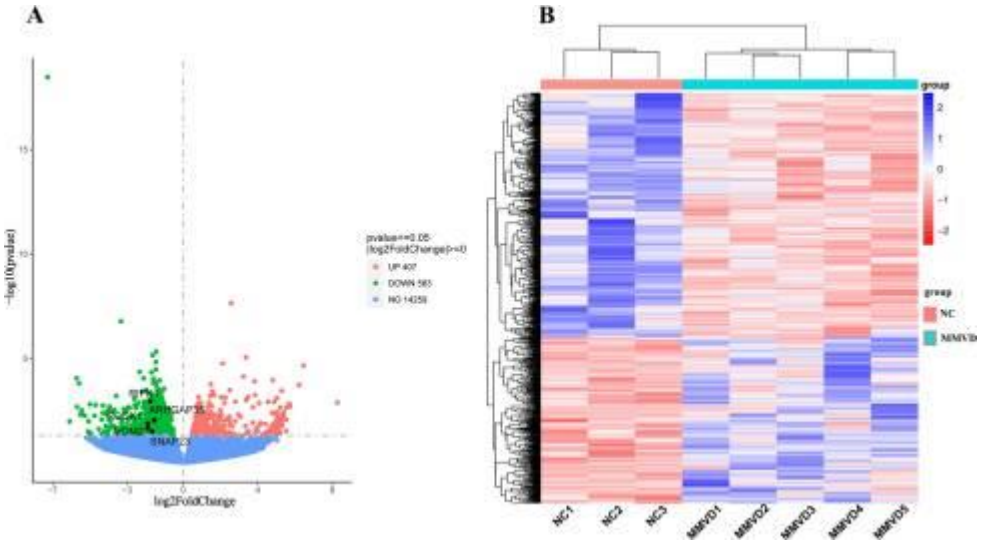

Figure 3. Detection and visualization of DEGs

A Volcano plot illustrating differential gene expression between NC and MMVD groups. The x-axis shows log2 fold changes, while the y-axis reflects the statistical significance of those changes. Each point corresponds to a single gene: red indicates significantly upregulated genes, green denotes significantly downregulated genes, and blue represents genes without significant expression shifts.

B Heatmap displaying hierarchical clustering of DEGs. Rows correspond to individual genes and columns represent samples. The color gradient (log2FC scale) ranges from red for higher expression to blue for lower expression.

Functional enrichment analysis of DEGs

To clarify the biological relevance of the identified DEGs, Gene Ontology (GO) enrichment analysis was performed. Among the enriched categories, phosphorylation (GO:0016310; 40 DEGs) was most represented within biological processes, nuclear components (GO:0005634; 26 DEGs) dominated the cellular component category, and DNA-binding activity (GO:0003677; 41 DEGs) was the most abundant molecular function **(Figure 4A)**. All enriched terms met the significance threshold of $P < 0.05$.

The top 20 GO terms enriched by DEGs are summarized in **Figure 4B**. The most strongly enriched molecular function terms were ubiquitin-protein transferase activity (GO:0004882; $P = 7.68\times10^{-5}$; 10 DEGs) and ubiquitin-like protein transferase activity (GO:0019787; $P = 7.68\times10^{-5}$; 10 DEGs). These terms were driven by the same set of 10 genes, including *HERC3*, *MSL2*, *UBR5*, *TRIP12*, *UBE3A*, *UBE4A*, among others, all of which encode enzymes involved in ubiquitin or ubiquitin-like protein transfer.

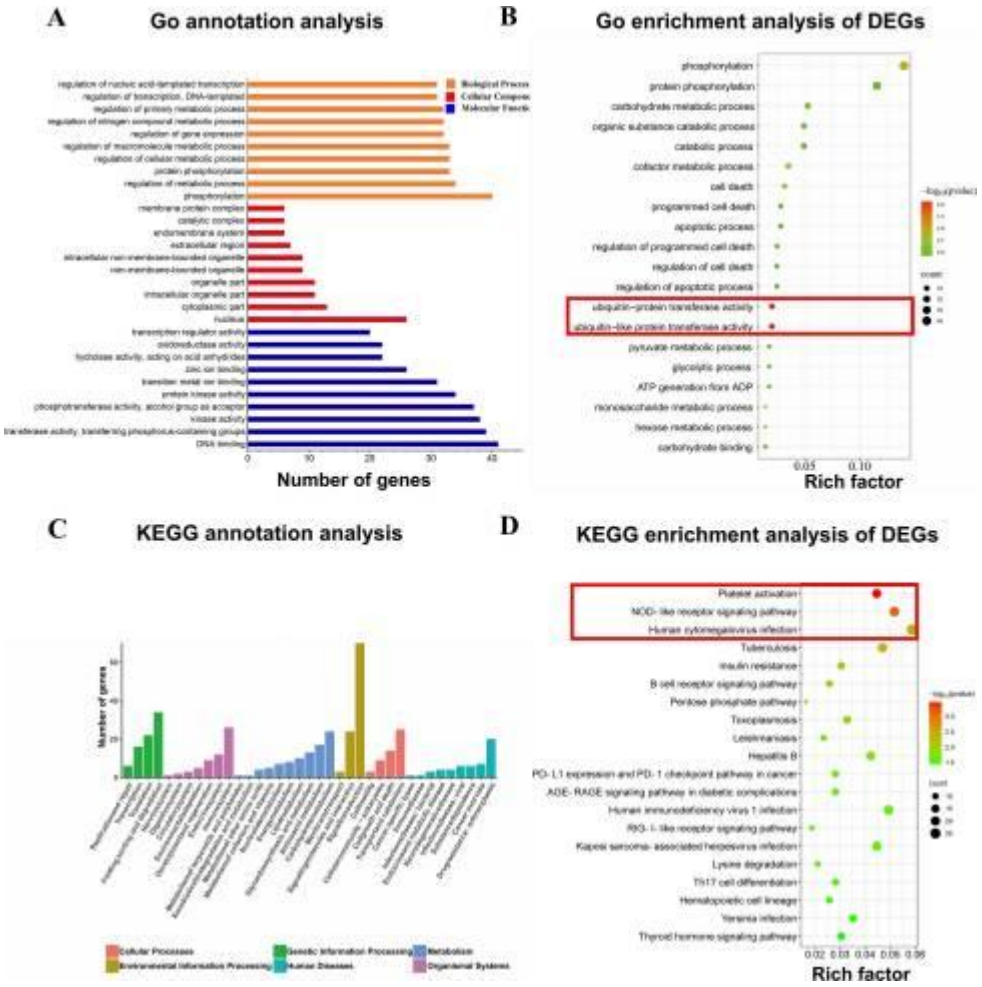

Figure 4. GO and KEGG enrichment analyses and Venn diagram of candidate genes

Panel A shows GO enrichment of the DEGs, with the x-axis representing the top 10 GO terms and the y-axis indicating their statistical significance. Biological processes (BP) are shown in red, cellular components (CC) in green, and molecular functions (MF) in blue. Panel B displays the 20 most enriched GO terms in dogs with MMVD. Panel C summarizes KEGG pathway classifications for the 990 DEGs, while Panel D highlights the 20 pathways with the highest enrichment.

KEGG pathway enrichment

KEGG annotation of the 990 DEGs allowed identification of the pathways in which these genes are involved. Among broad functional categories, signal transduction (70 DEGs) accounted for the largest proportion of environmental information processing, folding, sorting, and degradation (34 DEGs) dominated genetic information processing, and the immune system (26 DEGs) was the most represented within organismal systems **(Figure 4C)**. Overall, 286 KEGG pathways were mapped, and the top 20 pathways with the strongest enrichment are presented in **Figure 4D**. The most significantly enriched pathways included platelet activation (KEGG: cfa04611, $P = 3.47\times10^{-4}$, 19 DEGs), the NOD-like receptor signaling pathway (KEGG: cfa04621, $P = 7.68\times10^{-4}$, 22 DEGs), and the human cytomegalovirus infection pathway (KEGG: cfa05163, $P = 2.01\times10^{-3}$, 25 DEGs). Integrating the GO and KEGG results highlighted five key functional pathways: ubiquitin-like protein transferase activity, ubiquitin-protein transferase activity, platelet activation, NOD-like receptor signaling, and human cytomegalovirus infection. Across these pathways, 64 DEGs were identified, of which 19 were upregulated and 45 were downregulated.

Candidate gene identification

To assess whether hub genes in the turquoise module overlapped with platelet activation-related DEGs, a Venn diagram was generated. Among the 100 hub genes, 66 also belonged to the DEGs, and five genes specifically overlapped with platelet activation-associated DEGs. These genes were MDM2 ($log_2FC = –1.94$, $P < 0.05$), ROCK1 ($log_2FC = –1.92$, $P < 0.05$), RIPK1 ($log_2FC = –1.79$, $P < 0.05$), SNAP23 ($log_2FC = –1.69$, $P < 0.05$), and ARHGAP35 ($log_2FC = –1.58$, $P < 0.05$). Based on these results, these five genes were selected as candidate biomarkers for subsequent experimental validation.

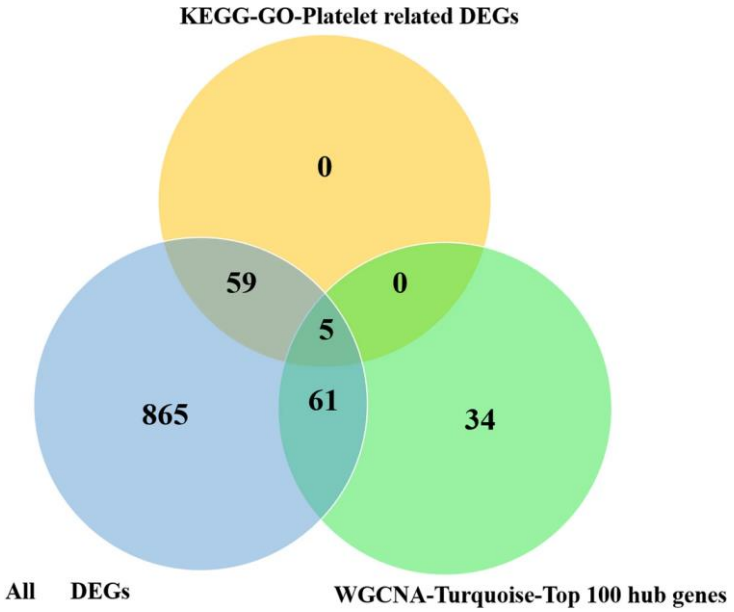

Figure 5. illustrates a Venn diagram showing the overlap among all DEGs, platelet activation-related DEGs identified through KEGG and GO analyses, and the top 100 hub genes from the turquoise module

RT-qPCR validation of transcriptome results

Based on the integrated results from differential expression analysis, functional enrichment (KEGG and GO), and WGCNA, five candidate genes—MDM2, ROCK1, RIPK1, SNAP23, and ARHGAP35—were selected for further validation due to their strong association with platelet activation pathways and echocardiographic parameters. Expression of these genes was assessed in a cohort of 108 dogs (52 NC, 56 MMVD) using RT-qPCR to confirm the RNA-seq findings. Statistically significant downregulation was observed for MDM2, ROCK1, RIPK1, and SNAP23 in MMVD dogs compared with controls ($P < 0.01$). Although ARHGAP35 was also downregulated, this change did not reach statistical significance ($P > 0.05$). Overall, the expression trends of these five candidate genes were consistent with the RNA-seq data **(Figure 6)**, supporting MDM2, ROCK1, RIPK1, and SNAP23 as potential biomarkers and therapeutic targets for MMVD.

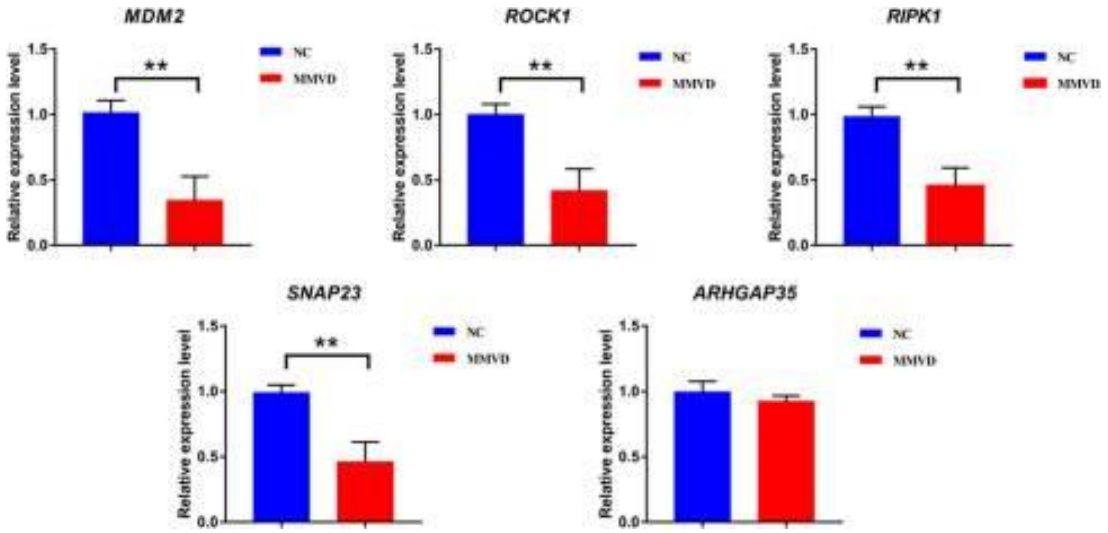

Figure 6. Real-time PCR validation of the candidate genes in the validation cohort. (**$P < 0.01$)

Correlation of candidate gene expression with radiographic parameters

To evaluate the relationship between the four candidate genes and cardiac structural changes, RT-qPCR expression levels in the validation cohort were correlated with radiographic measurements. MDM2, ROCK1, RIPK1, and SNAP23 all showed significant negative correlations with LA/AO, LVIDDN, and VHS ($P < 0.01$), as illustrated in **Figure 7**. Among these, LA/AO and LVIDDN exhibited the strongest association with MDM2, with a correlation coefficient of –0.89. In contrast, LA demonstrated only a moderate negative correlation with the four genes (correlation coefficients < –0.6), and no correlation was observed with AO. Overall, these findings largely mirrored the WGCNA results derived from the RNA-seq data, though the correlations with LA and AO were somewhat reduced in magnitude.

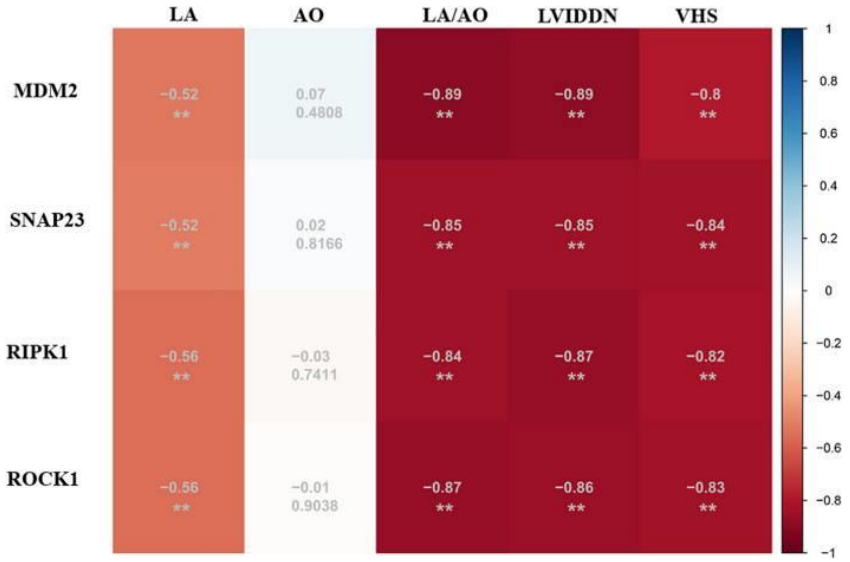

Figure 7. Correlation analysis between the radiology parameters and the candidate genes in the validation cohort (**$P < 0.01$)

Discussion

This study aimed to integrate RNA-seq with the systems biology approach of Weighted Gene Co-expression Network Analysis (WGCNA) to identify blood-based biomarkers associated with clinical features of MMVD stage B2, potentially informing diagnostic and therapeutic strategies. WGCNA is a widely used method for detecting clusters of highly co-expressed genes, forming modules, and assessing their relationships with specific traits [22]. To date, WGCNA has not been applied to MMVD, and in this study, it was employed to uncover genes

linked to cardiac remodeling and other clinical characteristics, providing a foundation for identifying novel biomarkers and therapeutic targets.

Transcriptomic profiling of eight blood samples—three from healthy controls and five from dogs with MMVD stage B2—resulted in the identification of 25,464 genes. Using WGCNA, these genes were organized into 41 co-expression modules. Analysis of module–trait relationships revealed that the turquoise module was most closely associated with key echocardiographic parameters, including LA, AO, LA:AO, and LVIDDN **(Figure 2C)**, with LA:AO showing the strongest correlation. LA:AO is a body size–independent and convenient index commonly used to assess left atrial enlargement in dogs with MMVD [8, 23], supporting the selection of the turquoise module for further analyses. Within this module, the top 100 hub genes, determined by intramodular connectivity (kWithin), were identified as closely linked to cardiac remodeling and used for subsequent investigations.

Differential expression analysis is a standard approach for exploring candidate biomarkers. Applying criteria of $|\log_2(\text{fold change})| > 0$ and $P < 0.05$, a total of 990 DEGs were identified, including 407 upregulated and 583 downregulated genes. Functional enrichment analysis using GO and KEGG revealed that these DEGs were significantly involved in platelet activation, NOD-like receptor signaling, human cytomegalovirus infection, and ubiquitin/ubiquitin-like protein transferase activity **(Figure 4B, D)**. In contrast, transcriptomic analyses of valvular tissue in dogs with MMVD have highlighted enrichment in epithelial-to-mesenchymal transition, basement membrane components, and TGF-β signaling [11–13, 24]. Nonetheless, inflammation, extracellular matrix organization, and platelet function-related pathways were enriched in both blood and tissue transcriptomes, suggesting that these processes are central to MMVD pathogenesis.

Platelet activation is functionally linked to NOD-like receptor signaling, human cytomegalovirus infection, and ubiquitin/ubiquitin-like protein transferase activity [25–27]. Among these, platelet-related pathways have garnered considerable attention due to their involvement in diverse cardiac disease processes [28, 29]. NOD-like receptor signaling has been shown to induce platelet activation during heatstroke and sepsis [25, 30]. Human cytomegalovirus directly modulates the platelet-derived growth factor system, and interactions between the virus and platelets trigger pro-inflammatory and pro-angiogenic responses, which exacerbate tissue damage and contribute to atherogenesis [31, 32]. Furthermore, extensive protein ubiquitylation occurs during platelet activation, highlighting the role of ubiquitin-mediated processes [33–35]. Collectively, these findings indicate that platelet activation-associated genes, intersecting with NOD-like signaling, cytomegalovirus-related pathways, and ubiquitin transferase activity, play a critical role in the progression of MMVD. Accordingly, DEGs enriched in these pathways were designated as platelet activation-related genes for downstream analysis.

Platelets are small, anucleate cells released from megakaryocytes into the bloodstream [36] and are critical contributors to cardiovascular pathology, including conditions such as atherosclerosis, myocardial infarction, and diabetic coronary artery disease [37–39]. In dogs with MMVD, turbulent high-speed blood flow and altered shear stress near the mitral valve leaflets have been implicated in triggering platelet activation [24, 28]. Supporting this notion, a recent proteomic study in dogs experiencing MMVD-related acute congestive heart failure found that the majority (60%) of platelet proteins were downregulated [28]. Similarly, our analysis revealed that 45 of 64 platelet activation-associated DEGs (approximately 70%) were reduced in expression in MMVD dogs, suggesting a notable suppression of platelet-related gene activity. Larger-scale studies are necessary to clarify the mechanisms underlying this downregulation.

Within the top 100 hub genes of the turquoise module, five genes—MDM2, ROCK1, RIPK1, SNAP23, and ARHGAP35—were linked to multiple platelet-associated biological pathways. The combined RNA-seq and network analyses indicate that platelet-related molecular processes may play a key role in the pathophysiology and potential diagnosis of MMVD stage B2.

The proto-oncogene MDM2 encodes a RING-type E3 ubiquitin ligase [40]. In oncology, MDM2 has been shown to promote tumor cell proliferation by activating platelet-derived growth factor signaling and modulating ubiquitination, and is overexpressed in soft-tissue sarcomas including osteosarcoma [41], retroperitoneal liposarcoma [42], and other liposarcomas [43]. Antagonism of MDM2 in cancer patients frequently results in thrombocytopenia [44–46]. In certain breeds predisposed to MMVD, such as Cavalier King Charles Spaniels and Maltese, low platelet counts are considered an inherited trait, potentially contributing to early disease onset [47, 48]. In the present study, MDM2 expression was markedly lower in dogs with MMVD stage B2 compared to controls, and negatively correlated with LA:AO, LVIDDN, and VHS (correlation coefficients = –0.89, –0.89, –0.80; $P < 0.01$) **(Figures 5–6)**. These findings highlight MDM2 as a promising biomarker and therapeutic

candidate, although the study did not measure platelet counts or functional status, leaving the link between reduced MDM2 expression and platelet physiology unresolved.

ROCK1, also referred to as Rho-kinase B, functions as a serine/threonine kinase and a downstream effector of RhoA GTPases [49]. RhoA signaling is critical for platelet regulation, mediating responses to vasoactive stimuli to maintain hemostasis and influencing cardiovascular disease progression [50, 51]. Inhibition of ROCK1/2 has been associated with increased megakaryocyte ploidy, aberrant proplatelet formation, and macrothrombocytopenia [52–54]. Interestingly, dogs with MMVD exhibiting macrothrombocytopenia also show increased left ventricular fractional shortening and reduced platelet activation, reflecting a hypercoagulable state [55]. In line with these findings, ROCK1 expression was significantly decreased in MMVD stage B2 dogs, suggesting that impaired ROCK1 may contribute to disease progression by limiting platelet activation.

Moreover, this study identified RIPK1 and SNAP23 as novel genes not previously studied in MMVD. RT-qPCR validation and correlation analyses confirmed their differential expression in stage B2 disease and a significant association with cardiac remodeling. These findings suggest that RIPK1 and SNAP23 represent new potential biomarkers and therapeutic targets for MMVD stage B2.

Study Limitations

Several limitations in this study should be acknowledged. First, the relatively small number of animals, especially in the discovery cohort, may reduce the reliability and generalizability of the results. This limitation may partly explain why ARHGAP35 was identified as differentially expressed in RNA-seq analysis but failed to reach significance in the validation cohort comprising multiple breeds. Second, the discovery cohort was restricted to a single breed (Poodles), which may limit the applicability of the findings to other dog breeds. Furthermore, this study represents an initial investigation into the genes associated with MMVD stage B2. More comprehensive analyses comparing healthy dogs with those at stages B1 and B2 are required to better understand stage-specific gene expression changes. Additionally, platelet counts and functional assays were not performed, leaving gaps in understanding how platelet-related hub genes influence disease progression. Future studies should explore the mechanistic roles of these hub genes in platelet activation and MMVD development both in vivo and in vitro.

Conclusions

This study demonstrates the utility of RNA-sequencing combined with systems-level bioinformatic analysis to identify gene networks linked to cardiac remodeling in MMVD stage B2. By applying WGCNA, we uncovered modules of co-expressed genes correlated with clinical echocardiographic parameters and highlighted hub genes involved in platelet activation pathways. To our knowledge, this is the first study to integrate WGCNA with clinical phenotypes in dogs with MMVD stage B2. Importantly, four candidate genes—MDM2, ROCK1, RIPK1, and SNAP23—were identified and validated as differentially expressed. While these genes have recognized roles in human cardiovascular diseases such as chronic heart failure, atherosclerosis, and diabetic cardiomyopathy, their involvement in MMVD has not been previously reported. The present findings provide a foundation for future research into the mechanistic contribution of these genes to MMVD pathogenesis and their potential as biomarkers or therapeutic targets.

Animals and blood sampling

This study involved canine patients presented at the Veterinary Medical Teaching Hospital of Huazhong Agricultural University (Wuhan, China) between August 2020 and December 2021. No animals were euthanized for research purposes. Blood samples were collected after obtaining written informed consent from the owners, and all procedures were approved by the Huazhong Agricultural University Animal Care and Use Committee (HZAUMO-2015–12). Following sample collection and clinical evaluation, the dogs were returned to their owners.

Based on the ACVIM consensus guidelines for canine myxomatous mitral valve disease (MMVD), 118 dogs were initially screened and assigned to either the healthy control group (NC) or the naturally occurring MMVD stage B2 group. Two dogs were excluded due to aggressive behavior during sampling. The study included a discovery cohort consisting of three NC Poodles and five MMVD stage B2 Poodles, and a validation cohort including 52

NC and 56 MMVD stage B2 dogs from multiple breeds. Healthy controls exhibited no abnormal findings on physical examination, radiography, echocardiography, or laboratory tests.
Dogs in the MMVD stage B2 group met all of the following: (1) a cardiac murmur intensity of ≥ 3/6, (2) left atrial to aortic ratio (LA:AO) ≥ 1.6 measured via right-sided short-axis echocardiography, (3) vertebral heart size (VHS) > 10.5 on radiographs, and (4) left ventricular internal diameter normalized to body weight ≥ 1.7. Exclusion criteria included severe systemic disease (liver, kidney, lung, or other organs), malignancy, recent medication use within 30 days, or aggressive behavior. Echocardiographic parameters were averaged across three consecutive cardiac cycles. Two board-certified veterinary radiologists, blinded to the group allocation, independently reviewed all imaging data.
Blood was collected from the jugular vein into EDTA tubes and immediately mixed with TRIzol reagent (Ambion, Thermo Fisher Scientific, USA) at a 1:3 ratio. Samples were agitated until the floccules disappeared, incubated at room temperature for 10 minutes, and stored at −80°C. All analyses were completed within one year of collection.

RNA extraction and library construction
Total RNA was isolated according to the manufacturer's protocol using TRIzol. RNA integrity and concentration were assessed on a Bioanalyzer 2100 with an RNA Nano 6000 Assay Kit (Agilent Technologies, CA, USA) [56]. Polyadenylated mRNA was purified from total RNA using magnetic beads with oligo(dT) primers. RNA fragments were generated via divalent cation-mediated cleavage at elevated temperature. First-strand cDNA synthesis employed random hexamer primers and M-MuLV Reverse Transcriptase, followed by degradation of RNA with RNase H. Second-strand synthesis was performed with DNA Polymerase I and dNTPs, and resulting overhangs were converted to blunt ends. After adenylation at the 3' ends, adaptors containing hairpin loops were ligated. Fragments ranging from 370 to 420 bp were selected with AMPure XP beads (Beckman Coulter, USA), amplified by PCR, and purified using the same system. Libraries were quantified using a Qubit 2.0 Fluorometer, diluted to 1.5 ng/μL, and fragment size validated on an Agilent 2100 Bioanalyzer. Paired-end sequencing (150 cycles) was performed on a NovaSeq 6000 platform (Illumina, USA) [57].

Genome alignment and gene annotation
Quality control of raw sequencing reads was performed using in-house Perl scripts, removing reads containing adapters, reads with N bases, and low-quality reads. Metrics including Q20, Q30, and GC content were calculated for the filtered clean reads [58]. The Canis lupus familiaris reference genome (http://asia.ensembl.org/Canis_lupus_familiaris/Info/Index) was indexed using Hisat2 (v2.0.5), and paired-end reads were aligned to the reference genome with the same software. Assembled transcripts for each sample were generated using StringTie v1.3.3b, allowing for novel transcript prediction. Gene-level read counts were obtained using FeatureCounts v1.5.0-p3, and functional annotation was performed using BLAST against GO and KEGG databases.

Gene expression quantification and DEG identification
FeatureCounts was used to quantify the reads mapped to each gene. Gene expression levels were calculated as FPKM (Fragments Per Kilobase of transcript per Million mapped reads), accounting for both gene length and sequencing depth [59]. Differential expression analysis between NC and MMVD groups was performed using the DESeq2 R package (v1.20.0), which models count data with a negative binomial distribution. P-values were adjusted for multiple testing using the Benjamini–Hochberg procedure. Genes with an adjusted P-value ≤ 0.05 and |log2 fold change| ≥ 0 were considered significantly differentially expressed [60].

Clustering of differentially expressed genes
FPKM values were log-transformed to approximate a normal distribution. Euclidean distances between all transformed data points were calculated, and hierarchical clustering was performed using the complete linkage method. Initially, each data point was treated as a separate cluster, and the two closest clusters were iteratively merged based on the shortest inter-cluster distance until all points formed a single hierarchical structure.

Functional enrichment analysis

GO term and KEGG pathway enrichment analyses of DEGs were conducted using the clusterProfiler R package (v3.8.1). Terms or pathways with adjusted P-values < 0.05 were considered significantly enriched. The most significant GO categories and KEGG pathways were selected according to their enrichment scores.

Weighted Gene Co-expression Network Analysis (WGCNA)
All 25,464 identified genes were used for WGCNA to identify modules associated with clinical traits. Expression values (FPKM) were used as input for the analysis. The R package WGCNA was used to construct co-expression networks, setting the soft-thresholding power to 10 (scale-free $R^2 = 0.70$) and the minimum module size to 10 genes. Modules showing the strongest correlations with clinical features were identified, and hub genes were defined as genes with high module membership (KME) values.

Validation of Candidate Genes by RT-qPCR
Total RNA was extracted with TRIzol (Invitrogen, USA) and reverse transcribed into cDNA using HiScript II Reverse Transcriptase (Vazyme, Nanjing, China). RT-qPCR was performed on a StepOne Plus system (Roche LightCycler@96, USA) using SYBR Green Master Mix. Relative expression levels were normalized to GAPDH using the 2^-ΔΔCt method. Primers were designed with Primer Premier 5.0.

Statistical analysis
All analyses were conducted in GraphPad Prism v8.0.2. Data are presented as mean ± SEM. Comparisons between groups were performed using unpaired Student's t-tests. A two-sided P-value < 0.05 was considered statistically significant. All experiments were repeated in triplicate.

Abbreviations

MMVD=Myxomatous mitral valve disease
cTNI=Cardiac troponin-I
DEGs=Differentially expressed genes
WGCNA=Weighted gene co-expression network analyses
LA:AO=Ratio of left atrium to aortic internal diameter in right-sided short axis view in early diastole
LVIDDN=Left ventricular internal diameter in diastole, normalized for body weight
NT-ProBNP=Natriuretic peptides
VHS=Radiographic vertebral heart score
MDM2=MDM2 proto-oncogene
ROCK1=Rho associated coiled-coli containing protein kinase 1
RIPK1=Receptor interacting serine/threonine kinase 1
SNAP23=Synaptosome associated protein 23
ARHGAP35=Rho GTPase activating protein 35

Acknowledgments: The authors thank all staff of Huazhong Agricultural University's Veterinary Medical Teaching Hospital that have took part in the collection of clinical data and analysis of samples for the study.

Conflict of Interest: None

Financial Support: This study was supported by a grant from the National Natural Science Foundation of China [Grant No. 31972744].

Ethics Statement: All animal experiments were performed according to protocols and guidelines approved by the Huazhong Agriculture University Animal Care and Use Committee (Wuhan, China). Written informed consent was obtained from each owner of the participating dogs.

References

1. Kim HS, Kang JH, Jeung EB, Yang MP. Serum concentrations of leptin and adiponectin in dogs with Myxomatous mitral valve disease. J Vet Intern Med. 2016;30(5):1589–600. doi: 10.1111/jvim.14570.
2. Poad MH, Manzi TJ, Oyama MA, Gelzer AR. Utility of radiographic measurements to predict echocardiographic left heart enlargement in dogs with preclinical myxomatous mitral valve disease. J Vet Intern Med. 2020;34(5):1728–33. doi: 10.1111/jvim.15854.
3. DeProspero DJ, O'Donnell KA, DeFrancesco TC, Keene BW, Tou SP, Adin DB, et al. Myxomatous mitral valve disease in Miniature Schnauzers and Yorkshire Terriers: 134 cases (2007–2016). J Am Vet Med Assoc. 2021;259(12):1428–32. doi: 10.2460/javma.20.05.0291.
4. Coffman M, Guillot E, Blondel T, Garelli-Paar C, Feng S, Heartsill S, et al. Clinical efficacy of a benazepril and spironolactone combination in dogs with congestive heart failure due to myxomatous mitral valve disease: the BESST study. J Vet Intern Med. 2021;35(4):1673–87. doi: 10.1111/jvim.16155
5. Häggström J, Boswood A, O'Grady M, Jöns O, Smith S, Swift S, et al. Effect of pimobendan or benazepril hydrochloride on survival times in dogs with congestive heart failure caused by naturally occurring myxomatous mitral valve disease: the QUEST study. J Vet Intern Med. 2008;22(5):1124–35. doi: 10.1111/j.1939-1676.2008.0150.x.
6. Jafar N, Moses MJ, Benenstein RJ, Vainrib AF, Slater JN, Tran HA, et al. 3D transesophageal echocardiography and radiography of mitral valve prostheses and repairs. Echocardiography. 2017;34(11):1687–701. doi: 10.1111/echo.13656.
7. Yang S, Lei S, Peng F, Wu SJ. Detection of pulmonary hypertension by combining echocardiography and chest radiography. Acad Radiol. 2022;29(Suppl 2):S23–S30. doi: 10.1016/j.acra.2020.10.003.
8. Keene BW, Atkins CE, Bonagura JD, Fox PR, Haggstrom J, Fuentes VL, et al. ACVIM consensus guidelines for the diagnosis and treatment of myxomatous mitral valve disease in dogs. J Vet Intern Med. 2019;33(3):1127–40. doi: 10.1111/jvim.15488.
9. Vezzosi T, Grosso G, Tognetti R, Meucci V, Patata V, Marchesotti F, et al. The Mitral INsufficiency Echocardiographic score: a severity classification of myxomatous mitral valve disease in dogs. J Vet Intern Med. 2021;35(3):1238–44. doi: 10.1111/jvim.16131
10. Wolf J, Gerlach N, Weber K, Klima A, Wess G. The diagnostic relevance of NT-proBNP and proANP 31–67 measurements in staging of myxomatous mitral valve disease in dogs. Vet Clin Pathol. 2013;42(2):196–206. doi: 10.1111/vcp.12044
11. Markby GR, Macrae VE, Summers KM, Corcoran BM. Disease severity-associated gene expression in canine myxomatous mitral valve disease is dominated by TGFβ signaling. Front Genet. 2020;11:372. doi: 10.3389/fgene.2020.00372
12. Lu CC, Liu MM, Culshaw G, Clinton M, Argyle DJ, Corcoran BM. Gene network and canonical pathway analysis in canine myxomatous mitral valve disease: a microarray study. Vet J. 2015;204(1):23–31. doi: 10.1016/j.tvjl.2015.02.021
13. Lu CC, Liu MM, Clinton M, Culshaw G, Argyle DJ, Corcoran BM. Developmental pathways and endothelial to mesenchymal transition in canine myxomatous mitral valve disease. Vet J. 2015;206(3):377–84. doi: 10.1016/j.tvjl.2015.08.011.
14. Guo F, Zhang B, Yang H, Fu Y, Wang Y, Huang J, et al. Systemic transcriptome comparison between early- and late-onset pre-eclampsia shows distinct pathology and novel biomarkers. Cell Prolif. 2021;54(2):e12968. doi: 10.1111/cpr.12968
15. Tvarijonaviciute A, Ceron JJ, Martinez-Subiela S, García-Martinez JD. Serum and urinary adiponectin in dogs with renal disease from leishmaniasis. Vet Rec. 2012;171(12):297. doi: 10.1136/vr.100855
16. Gong X, Zheng M, Zhang J, Ye Y, Duan M, Chamba Y, et al. Transcriptomics-based study of differentially expressed genes related to fat deposition in Tibetan and Yorkshire pigs. Front Vet Sci. 2022;9:919904. doi: 10.3389/fvets.2022.919904.
17. Yang J, Chen X, Zhu C, Peng X, He X, Fu J, et al. Using RNA-seq to profile gene expression of spikelet development in response to temperature and nitrogen during meiosis in rice (Oryza sativa L.). PLoS One. 2015;10(12):e0145532. doi: 10.1371/journal.pone.0145532.
18. He Q, Lin Y, Tan H, Zhou Y, Wen Y, Gan J, et al. Transcriptomic profiles of Dunaliella salina in response to hypersaline stress. BMC Genomics. 2020;21(1):115. doi: 10.1186/s12864-020-6507-2.

19. Song ZY, Chao F, Zhuo Z, Ma Z, Li W, Chen G. Identification of hub genes in prostate cancer using robust rank aggregation and weighted gene co-expression network analysis. Aging (Albany NY). 2019;11(13):4736–56. doi: 10.18632/aging.102087.
20. Liu Z, Ma C, Gu J, Yu M. Potential biomarkers of acute myocardial infarction based on weighted gene co-expression network analysis. Biomed Eng Online. 2019;18(1):9. doi: 10.1186/s12938-019-0625-6.
21. Chen Q, Su L, Liu C, Gao F, Chen H, Yin Q, et al. PRKAR1A and SDCBP serve as potential predictors of heart failure following acute myocardial infarction. Front Immunol. 2022;13:878876. doi: 10.3389/fimmu.2022.878876.
22. Langfelder P, Horvath S. WGCNA: an R package for weighted correlation network analysis. BMC Bioinformatics. 2008;9:559. doi: 10.1186/1471-2105-9-559
23. Hsue W, Visser LC. Reproducibility of echocardiographic indices of left atrial size in dogs with subclinical myxomatous mitral valve disease. J Vet Intern Med. 2020;34(5):1779–86. doi: 10.1111/jvim.15850.
24. Moesgaard SG, Sørensen TM, Sterup A, Tarnow I, Kristensen AT, Jensen AL, et al. Changes in platelet function in Dachshunds with early stages of myxomatous mitral valve disease. Res Vet Sci. 2009;86(2):320–4. doi: 10.1016/j.rvsc.2008.07.019.
25. Zhong H, Waresi M, Zhang W, Han L, Zhao Y, Chen Y, et al. NOD2-mediated P2Y(12) upregulation increases platelet activation and thrombosis in sepsis. Biochem Pharmacol. 2021;194:114822. doi: 10.1016/j.bcp.2021.114822.
26. Soroceanu L, Akhavan A, Cobbs CS. Platelet-derived growth factor-alpha receptor activation is required for human cytomegalovirus infection. Nature. 2008;455(7211):391–5. doi: 10.1038/nature07209.
27. Kasirer-Friede A, Tjahjono W, Eto K, Shattil SJ. SHARPIN at the nexus of integrin, immune, and inflammatory signaling in human platelets. Proc Natl Acad Sci U S A. 2019;116(11):4983–8. doi: 10.1073/pnas.181915611.
28. Levent P, Kocaturk M, Akgun E, Saril A, Cevik O, Baykal AT, et al. Platelet proteome changes in dogs with congestive heart failure. BMC Vet Res. 2020;16(1):466. doi: 10.1186/s12917-020-02692-x
29. Mauler M, Herr N, Schoenichen C, Witsch T, Marchini T, Härdtner C, et al. Platelet serotonin aggravates myocardial ischemia/reperfusion injury via neutrophil degranulation. Circulation. 2019;139(7):918–31. doi: 10.1161/CIRCULATIONAHA.118.033942.
30. Yin H, Wu M, Lu Y, Wu X, Yu B, Chen R, et al. HMGB1-activated NLRP3 inflammasome induces thrombocytopenia in heatstroke rat. PeerJ. 2022;10:e13799. doi: 10.7717/peerj.13799.
31. Assinger A, Kral JB, Yaiw KC, Schrottmaier WC, Kurzejamska E, Wang Y, et al. Human cytomegalovirus-platelet interaction triggers toll-like receptor 2-dependent proinflammatory and proangiogenic responses. Arterioscler Thromb Vasc Biol. 2014;34(4):801–9. doi: 10.1161/ATVBAHA.114.303287
32. Reinhardt B, Mertens T, Mayr-Beyrle U, Frank H, Lüske A, Schierling K, et al. HCMV infection of human vascular smooth muscle cells leads to enhanced expression of functionally intact PDGF beta-receptor. Cardiovasc Res. 2005;67(1):151–160. doi: 10.1016/j.cardiores.2005.03.012.
33. Unsworth AJ, Bombik I, Pinto-Fernandez A, McGouran JF, Konietzny R, Zahedi RP, et al. Human platelet protein ubiquitylation and changes following GPVI activation. Thromb Haemost. 2019;119(1):104–16. doi: 10.1055/s-0038-1676344.
34. Zhou Y, Abraham S, Renna S, Edelstein LC, Dangelmaier CA, Tsygankov AY, et al. TULA-2 (T-Cell Ubiquitin Ligand-2) inhibits the platelet Fc receptor for IgG IIA (FcγRIIA) signaling pathway and heparin-induced thrombocytopenia in mice. Arterioscler Thromb Vasc Biol. 2016;36(12):2315–23. doi: 10.1161/ATVBAHA.116.307979.
35. Rorsman C, Tsioumpekou M, Heldin CH, Lennartsson J. The ubiquitin ligases c-Cbl and Cbl-b negatively regulate platelet-derived growth factor BB-induced chemotaxis by affecting PDGFRβ internalization and signaling. J Biol Chem. 2016;291(22):11608–18. doi: 10.1074/jbc.M115.705814.
36. Montenont E, Echagarruga C, Allen N, Araldi E, Suarez Y, Berger JS, et al. Platelet WDR1 suppresses platelet activity and is associated with cardiovascular disease. Blood. 2016;128(16):2033–42. doi: 10.1182/blood-2016-03-703157.
37. Qi Z, Hu L, Zhang J, Yang W, Liu X, Jia D, et al. PCSK9 (Proprotein Convertase Subtilisin/Kexin 9) enhances platelet activation, thrombosis, and myocardial infarct expansion by binding to platelet CD36. Circulation. 2021;143(1):45–61. doi: 10.1161/CIRCULATIONAHA.120.046290.

38. Sun XD, Han L, Lan HT, Qin RR, Song M, Zhang W, et al. Endothelial microparticle-associated protein disulfide isomerase increases platelet activation in diabetic coronary heart disease. Aging (Albany NY). 2021;13(14):18718–39. doi: 10.18632/aging.203316.
39. Bakogiannis C, Sachse M, Stamatelopoulos K, Stellos K. Platelet-derived chemokines in inflammation and atherosclerosis. Cytokine. 2019;122:154157. doi: 10.1016/j.cyto.2017.09.013.
40. Jean-Charles PY, Yu SM, Abraham D, Kommaddi RP, Mao L, Strachan RT, et al. Mdm2 regulates cardiac contractility by inhibiting GRK2-mediated desensitization of β-adrenergic receptor signaling. JCI Insight. 2017;2(17):e95998. doi: 10.1172/jci.insight.95998.
41. Bouaoud J, Larousserie F, Galmiche-Rolland L, Bouvier C, Picard A, Khonsari RH. Protuberant fibro-osseous lesion of the temporal bone: report of four cases and review of the literature. Int J Oral Maxillofac Surg. 2021;50(12):1566–70. doi: 10.1016/j.ijom.2021.03.002.
42. Casadei L, de Faria FCC, Lopez-Aguiar A, Pollock RE, Grignol V. Targetable pathways in the treatment of retroperitoneal liposarcoma. Cancers (Basel). 2022;14(6):1362. doi: 10.3390/cancers14061362.
43. Thirasastr P, Somaiah N. Overview of systemic therapy options in liposarcoma, with a focus on the activity of selinexor, a selective inhibitor of nuclear export in dedifferentiated liposarcoma. Ther Adv Med Oncol. 2022;14:17588359221081073. doi: 10.1177/17588359221081073.
44. Takahashi S, Fujiwara Y, Nakano K, Shimizu T, Tomomatsu J, Koyama T, et al. Safety and pharmacokinetics of milademetan, a MDM2 inhibitor, in Japanese patients with solid tumors: a phase I study. Cancer Sci. 2021;112(6):2361–70. doi: 10.1111/cas.14875.
45. de Weger VA, de Jonge M, Langenberg MHG, Schellens JHM, Lolkema M, Varga A, et al. A phase I study of the HDM2 antagonist SAR405838 combined with the MEK inhibitor pimasertib in patients with advanced solid tumours. Br J Cancer. 2019;120(3):286–93. doi: 10.1038/s41416-018-0355-8.
46. Patnaik A, Tolcher A, Beeram M, Nemunaitis J, Weiss GJ, Bhalla K, et al. Clinical pharmacology characterization of RG7112, an MDM2 antagonist, in patients with advanced solid tumors. Cancer Chemother Pharmacol. 2015;76(3):587–95. doi: 10.1007/s00280-015-2830-8.
47. Reimann MJ, Fredholm M, Cremer SE, Christiansen LB, Meurs KM, Møller JE, et al. Polymorphisms in the serotonin transporter gene and circulating concentrations of neurotransmitters in Cavalier King Charles Spaniels with myxomatous mitral valve disease. J Vet Intern Med. 2021;35(6):2596–606. doi: 10.1111/jvim.16277.
48. Höglund K, Häggström J, Hanås S, Merveille AC, Gouni V, Wiberg M, et al. Interbreed variation in serum serotonin (5-hydroxytryptamine) concentration in healthy dogs. J Vet Cardiol. 2018;20(4):244–53. doi: 10.1016/j.jvc.2018.05.002.
49. Hsu LW, Chen PW, Chang WT, Lee WH, Liu PY. The role of ROCK in platelet-monocyte collaborative induction of thromboinflammation during acute coronary syndrome. Thromb Haemost. 2020;120(10):1417–31. doi: 10.1055/s-0040-1714278.
50. Shimokawa H, Sunamura S, Satoh K. RhoA/Rho-Kinase in the cardiovascular system. Circ Res. 2016;118(2):352–66. doi: 10.1161/CIRCRESAHA.115.306532.
51. Aslan JE. Platelet Rho GTPase regulation in physiology and disease. Platelets. 2019;30(1):17–22. doi: 10.1080/09537104.2018.1475632.
52. O'Sullivan LR, Cahill MR, Young PW. The importance of Alpha-Actinin proteins in platelet formation and function, and their causative role in congenital macrothrombocytopenia. Int J Mol Sci. 2021;22(17):9363. doi: 10.3390/ijms22179363.
53. Donada A, Balayn N, Sliwa D, Lordier L, Ceglia V, Baschieri F, et al. Disrupted filamin A/α(IIb)β(3) interaction induces macrothrombocytopenia by increasing RhoA activity. Blood. 2019;133(16):1778–88. doi: 10.1182/blood-2018-07-861427.
54. Ito Y, Nakamura S, Sugimoto N, Shigemori T, Kato Y, Ohno M, et al. Turbulence activates platelet biogenesis to enable clinical scale ex vivo production. Cell. 2018;174(3):636–48.e618. doi: 10.1016/j.cell.2018.06.011.
55. Öberg J, Lilliehöök I, Höglund K, Ljungvall I. Hemostatic function in Cavalier King Charles Spaniels assessed using thromboelastography. Vet Clin Pathol. 2019;48(4):636–44. doi: 10.1111/vcp.12795.
56. Kiewe P, Gueller S, Komor M, Stroux A, Thiel E, Hofmann WK. Prediction of qualitative outcome of oligonucleotide microarray hybridization by measurement of RNA integrity using the 2100 Bioanalyzer capillary electrophoresis system. Ann Hematol. 2009;88(12):1177–83. doi: 10.1007/s00277-009-0751-5.

57. Park YS, Kim S, Park DG, Kim DH, Yoon KW, Shin W, et al. Comparison of library construction kits for mRNA sequencing in the Illumina platform. Genes Genomics. 2019;41(10):1233–40. doi: 10.1007/s13258-019-00853-3.
58. Armstrong J, Fiddes IT, Diekhans M, Paten B. Whole-genome alignment and comparative annotation. Annu Rev Anim Biosci. 2019;7:41–64. doi: 10.1146/annurev-animal-020518-115005.
59. Jiang L, Schlesinger F, Davis CA, Zhang Y, Li R, Salit M, et al. Synthetic spike-in standards for RNA-seq experiments. Genome Res. 2011;21(9):1543–51. doi: 10.1101/gr.121095.111.
60. Hansen KD, Brenner SE, Dudoit S. Biases in Illumina transcriptome sequencing caused by random hexamer priming. Nucleic Acids Res. 2010;38(12):e131. doi: 10.1093/nar/gkq224.